



Full length article

Revisiting thermal transport in ThO₂ using higher-order thermal transport physicsNidheesh Virakante^{ID}, Ankit Jain^{ID *}

Department of Mechanical Engineering, IIT Bombay, Mumbai, 400076, India

ARTICLE INFO

Keywords:

ThO₂
Phonon thermal transport
First-principles
Lattice dynamics
Lattice thermal conductivity

ABSTRACT

The effect of inclusion of higher-order thermal transport physics (viz. temperature-dependent interatomic force constants, phonon renormalization, and four-phonon scattering) on the computation of phonon frequencies and lattice thermal conductivity of ThO₂ is explored, employing LDA, PBE, and PBEsol exchange-correlational functionals. Upon renormalization, the frequencies are stiffened for the optical phonon modes, whereas the acoustic modes remain unchanged. Thermal conductivity computed using LDA and PBEsol functionals are within 5% of the experimentally measured values at 300 K, whereas that obtained using PBE functional results in an underprediction of 25%. The temperature-dependent force constants and renormalized phonon frequencies significantly affect the computed lattice thermal conductivity at higher temperatures (40% difference at 1000 K), whereas four-phonon processes have minimal effects (only 10% at 1000 K).

1. Introduction

Nuclear energy is a carbon-free form of energy and is sought to play an important role in meeting our ever-increasing energy demand. Currently, uranium and its mixed oxides-based fuels are the choice of fuel in nuclear reactors worldwide. However, the focus is shifting to thorium-based fuels (such as ThO₂) owing to their desirable thermo-physical properties, higher radiation damage resistance, comparatively more natural abundance, and their higher resistance to nuclear proliferation [1–3]. Amongst other considerations, the efficient thermal energy transport inside nuclear fuel is one of the design considerations for the safety and efficiency of nuclear reactors [1,4,5]. Consequently, many research studies investigated thermal transport characteristics of ThO₂ [1,2,6–26].

From the experimental side, most past studies employed sintered/pressed pellets for studying thermal transport characteristics of ThO₂ owing to difficulties in growing single crystals [6–10]. With advances in chemical sciences, researchers recently successfully measured the thermal conductivity of large ThO₂ single crystals at and below room temperature [11,16]. The thermal conductivity is found to decrease with increasing temperature in the measured temperature range due to an increase in phonon scattering at higher temperatures [27,28]. The computational efforts based on lattice dynamics and the Boltzmann transport equation were initially limited to empirical interatomic forcefields [29–32]. While these empirical forcefield-driven calculations were able to correctly describe the phonon thermal conductivity

for most materials, they failed to describe optical phonon modes of ThO₂ [18,33].

Driven by the recent success of first-principles-driven lattice dynamics and Boltzmann transport equation (BTE)-based calculations in predicting phonon thermal transport properties of varying materials [34, 35], researchers also tested the applicability of these calculations for ThO₂ [2,12–23]. In particular, Zhang et al. [36] tested the validity of Hubbard-*U* correction in ThO₂ (owing to the over-screening of *d*- and *f*-band electrons in metal oxides by density functional theory (DFT)) and found that *U* or *J* corrections lead to incorrect results for ThO₂ [12, 13]. The vacant 5*f*-orbital (and absence of strong electron correlation effects) in ThO₂ makes it a suitable surrogate material for studying other actinide oxides [1,22]. Dennet et al. benchmarked the accuracy of different exchange correlational functionals (LDA, GGA-PW91, and SCAN) based on predicted phonon dispersion and concluded that LDA and SCAN functionals result in an agreement with experimentally measured phonon dispersion while GGA-PW91 functional results in an under-prediction of the optical phonon frequencies [16]. Consequently, LDA, SCAN (and PBEsol) functionals are majorly employed to study the thermal transport properties of ThO₂ [16,18,20–22], and the study of Nakamura and Machida [22] concluded no difference in obtained thermal conductivities between LDA and PBEsol functionals. All of these calculations, however, are based on the lowest-order thermal transport physics with no inclusion of phonon renormalization, higher-order four-phonon scattering, or temperature dependence of the potential

* Corresponding author.

E-mail address: a_jain@iitb.ac.in (A. Jain).

energy surface. As such, the obtained agreement between experimentally measured and LDA-based phonon dispersions, for instance, could change with the stiffening/softening of phonons owing to phonon renormalization. Wang et al. reported phonon dispersion and thermal conductivity of ThO_2 by accounting for phonon renormalization using the PBEsol functional, but the effect of phonon renormalization on functional benchmarking and the importance of higher-order phonon scattering and temperature-dependent potential energy surface were not studied [21]. In this work, we revisit first-principles-based thermal transport in ThO_2 by including the effect of phonon renormalization, four-phonon scattering, and the temperature-dependent sampling of the potential energy surface and study the accuracy of different functionals in describing thermal transport. For our study, we focused on the temperature range up to room temperature for which single-crystal experimental results are available. We find that with phonon renormalization, the optical modes in ThO_2 stiffens, while the acoustic modes remain unchanged. The thermal conductivities obtained using the PBE functional are 25% lower than the experimentally measured values (reported to be in the range 18–20 W/m·K at 300 K [11]) despite the overall good performance of PBE functional in describing the phonon dispersion, whereas those obtained with LDA and PBEsol functionals lie within 5% of the experimentally measured values.

2. Theory and methods

We obtain the lattice thermal conductivity, κ_α , of ThO_2 in the α -direction by solving the BTE along with the Fourier's law as [34,37–40]:

$$\kappa_\alpha = \sum_q \sum_v c_{qv} v_{qv,\alpha}^2 \tau_{qv}, \quad (1)$$

where the summation is over all the phonon modes, enumerated by wavevector q and mode v , c_{qv} is the phonon heat capacity, $v_{qv,\alpha}$ is the α component of phonon group velocity, ν_{qv} , and τ_{qv} is the phonon scattering lifetime. The phonon heat capacity is obtained by using the Bose-Einstein distribution ($c_{qv} = \frac{\hbar\omega_{qv}}{V} \frac{\partial n_{qv}^o}{\partial T}$) and the phonon group velocities are obtained from the slope of phonon dispersion relations ($v_{qv} = \frac{\partial \omega_{qv}}{\partial q}$), where \hbar is the reduced Planck constant, ω_{qv} is the phonon frequency, V is the crystal volume, and T is the temperature. The Bose-Einstein distribution, n_{qv}^o , is given by $n_{qv}^o = \frac{1}{\exp\left(\frac{\hbar\omega_{qv}}{k_B T}\right) - 1}$, where

k_B is the Boltzmann constant. The phonon frequencies are obtained by diagonalizing the dynamical matrix as $\omega_{qv}^2 e_{qv} = D_q \cdot e_{qv}$, with the elements of the Dynamical matrix obtained from:

$$D_q^{3(b-1)+\alpha,3(b'-1)+\beta} = \frac{1}{\sqrt{m_b m_{b'}}} \sum_{l'} \Phi_{b0;b'l'}^{\alpha\beta} \exp\{i[q \cdot (r_{b'l'} - r_{b0})]\}, \quad (2)$$

where the summation is over all unit-cells in the lattice, m_b is the mass of atom b in the unit-cell, r_{bl} is the position vector of atom b in the l th unit-cell, and $\Phi_{ij}^{\alpha\beta}$ is the real-space $(ij, \alpha\beta)$ -element of the harmonic force constant matrix Φ . The phonons defined at the harmonic level are eigenmodes of the system and are non-interacting. The phonon-phonon interactions are introduced (to obtain τ_{qv}) as perturbation using the Fermi-golden rule to obtain the phonon scattering rates via the three-phonon scattering processes as:

$$\frac{1}{\tau_{qv}^{3ph}} = \sum_{q_1 v_1} \sum_{q_2 v_2} \left\{ \left\{ (n_{q_1 v_1} - n_{q_2 v_2}) W^+ \right\} + \frac{1}{2} \left\{ (n_{q_1 v_1} - n_{q_2 v_2} + 1) W^- \right\} \right\}, \quad (3)$$

where W represents scattering probability matrix given by:

$$W^\pm = \frac{2\pi}{\hbar^2} \left| \Psi_{q(\pm q_1)(-q_2)}^{vv_1v_2} \right|^2 \delta(\omega_{qv} \pm \omega_{q_1 v_1} - \omega_{q_2 v_2}). \quad (4)$$

The $\Psi_{q_1 q_2}^{vv_1v_2}$ is the Fourier transform of real-space cubic constants ($\Psi_{bl;b'l';b''l''}^{\alpha\beta\gamma}$) and is obtained as:

$$\Psi_{q_1 q_2}^{vv_1v_2} = \Psi_{q_1' q_2'}^{vv'v''} = N \left(\frac{\hbar}{2N} \right)^{\frac{3}{2}} \sum_b \sum_{b'l'} \sum_{b''l''} \sum_{\alpha\beta\gamma} \Psi_{bl;b'l';b''l''}^{\alpha\beta\gamma} \times \frac{\tilde{e}_{b,qv}^\alpha \tilde{e}_{b',q'v'}^\beta \tilde{e}_{b'',q''v''}^\gamma}{\sqrt{m_b \omega_{qv} m_{b'} \omega_{q'v'} m_{b''} \omega_{q''v''}}} e^{i(q' \cdot r_{0l'} + q'' \cdot r_{0l''})}. \quad (5)$$

The summation in Eq. (5) is performed over phonon wavevectors satisfying crystal momentum conservation, i.e., $q + q_1 + q_2 = G$, where G is the reciprocal space lattice vector.

The methodology discussed so far is the lowest-order theory to obtain the phonon thermal conductivity of materials. While this theory has been shown to work well for a variety of materials, including simple and compound semiconductors, and an excellent agreement with experiments is obtained (where available) [41–44], this theory has recently been reported to result in an incomplete description of thermal transport physics in strongly anharmonic materials [45], at high-temperatures [46], and in ultra-high thermal conductivity materials due to the following reasons:

- 1. Quartic Phonon Renormalization:** The harmonic potential energy well experienced by atoms at finite temperatures is an average of thermally perturbed energy wells arising from the finite thermal displacements of atoms from their equilibrium positions. This could be accounted for in the dynamical matrix (Eq. (2)) by using the thermally averaged harmonic force constant as [45]:

$$\begin{aligned} \Phi_{ij}^{c,\alpha\beta} &= \frac{\partial^2 U}{\partial u_i^\alpha \partial u_j^\beta} \\ &= \Phi_{ij}^{o,\alpha\beta} + \frac{1}{2} \sum_{l''l'''l''''} \sum_{b''b'''b''''} \sum_{\gamma\delta} \Xi_{ijkl}^{\alpha\beta\gamma\delta} u_i^\alpha u_j^\beta \\ &= \Phi_{ij}^{o,\alpha\beta} + \frac{\hbar}{4N} \sum_{l''l'''l''''} \sum_{b''b'''b''''} \sum_{\gamma\delta} \sum_{qv} \Xi_{ijkl}^{\alpha\beta\gamma\delta} \\ &\quad \frac{\tilde{e}_{b''',qv}^\gamma \tilde{e}_{b''''qv}^\delta}{\omega_{qv} \sqrt{m_{b'''} m_{b''''}}} (2n_{qv} + 1) e^{i q \cdot (r_{0l'''} - r_{0l''''})}, \end{aligned} \quad (6)$$

where $\Phi_{ij}^{c,\alpha\beta}$ and $\Phi_{ij}^{o,\alpha\beta}$ are corrected and original harmonic force constants. Hereafter, the abbreviation ‘renorm’ is used while referring to quartic phonon renormalization.

- 2. Temperature-dependent Force Constants:** The interatomic force constants obtained using the static equilibrium structure of material fail to capture the temperature dependence of potential energy surface arising from the thermal population/perturbations of atoms at finite temperatures. This could be accounted for by sampling the potential energy surface at finite temperatures using either the molecular dynamics simulations or the thermal snapshot method. In the thermal snapshot method, instead of using the static equilibrium position of atoms, the thermally perturbed positions of atoms are used to obtain forces, which are subsequently fitted using the Taylor-series fit to obtain the temperature-dependent interatomic force constants [45,47]. The thermally perturbed positions of atoms are obtained from:

$$u_{b,l}^\alpha = \frac{1}{\sqrt{N}} \sum_{qv} \sqrt{\frac{\hbar(n_{qv} + 1)}{m_b \omega_{qv}}} \cos(2\pi\eta_{1,qv}) \sqrt{-\ln(1 - \eta_{2,qv})} \tilde{e}_{b,qv}^\alpha e^{i q \cdot r_{0l}}, \quad (7)$$

where $\eta_{1,qv}$ and $\eta_{2,qv}$ are random numbers sampled from a uniform distribution and constrained by $\eta_{1,qv} = \eta_{1,-qv}$ and $\eta_{2,qv} = \eta_{2,-qv}$. We perform Taylor-series fitting to obtain temperature-dependent cubic and quartic force constants by using residual forces obtained by removing the contribution of harmonic force

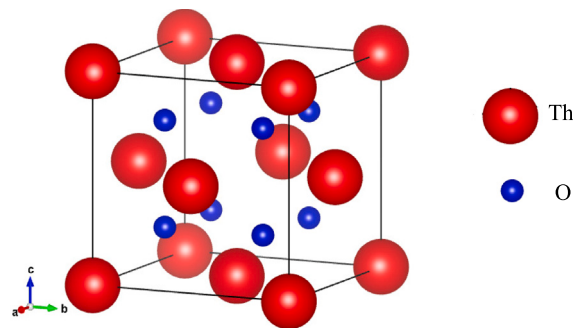


Fig. 1. Crystal Structure of ThO_2 . ThO_2 has fluorite structure-type with 12 atoms in the conventional unitcell.

constants. The effect of temperature on harmonic force constants is included via the use of temperature-dependent quartic force constants in the renormalization process (Eq. (6) above). Hereafter, the abbreviation ‘tdep’ is used while referring to temperature-dependent force constants.

- 3. Four-phonon Scattering:** The contribution from four-phonon processes could be significant in phonon–phonon interactions. This can be accounted for by obtaining the four-phonon scattering rates ($\frac{1}{\tau_{qv}^{4ph}}$) and combining them with the three-phonon scattering rates using the Matthiessen rule to obtain the effective scattering rate of phonon as:

$$\frac{1}{\tau_{qv}} = \frac{1}{\tau_{qv}^{3ph}} + \frac{1}{\tau_{qv}^{4ph}}. \quad (8)$$

Similar to three-phonon scattering rates, the four-phonon scattering rates can be obtained using the Fermi golden rule. Hereafter, the abbreviation ‘4ph’ [‘3ph’] is used while referring to four-phonon [three-phonon] scattering processes.

3. Computational details

The conventional unitcell of ThO_2 is composed of 12 atoms located at the FCC lattice sites in fluorite structure-type with three-atom basis [Th at (0,0,0) and O at (1/4,1/4,1/4), (3/4,3/4,3/4)], as shown in Fig. 1. The relaxed lattice structure (lattice constant) is obtained by performing energy minimization using periodic density functional theory (DFT) calculations as implemented in the quantum chemistry package Quantum Espresso [49,50]. The calculations are performed using plane wave basis set kinetic energy cutoff of 90 Ry and electronic wavevector grid of $8 \times 8 \times 8$ using the plane wave-based PAW pseudopotentials [51]. The harmonic interatomic force constants are obtained using the density functional perturbation theory (DFPT) [52]. The harmonic force constants are obtained originally on a coarser phonon wavevector grid of $8 \times 8 \times 8$ and are interpolated to a wavevector grid of size $20 \times 20 \times 20$ for phonon–phonon scattering rate calculations. The effect of long-range Coulombic interactions is considered via the non-analytical correction based on Born effective charges and dielectric constant (both obtained using the DFPT calculations). For anharmonic interatomic force constants, the obtained harmonic force constants are used to thermally populate 200 supercells of 192 atoms each, to obtain temperature-dependent perturbation of atoms using Eq. (7). The forces on these thermally perturbed cells are obtained using the DFT calculations with a Gamma-only sampling of the electronic Brillouin zone. The contribution of static harmonic force constants is removed from these forces, and the residual forces (along with known thermal perturbations) are fitted using the Taylor series to obtain the temperature-dependent cubic and quartic force constants. The interaction cutoffs for cubic and quartic force constants are set to 7.5 Å and

3.0 Å in this fitting procedure. The obtained temperature-dependent quartic force constants are used to obtain thermally averaged harmonic force constants for dynamical matrix calculations. The three-phonon and four-phonon scattering rates are obtained using an $20 \times 20 \times 20$ phonon wavevector grid and the relaxation time approximation of the BTE. Using only three-phonon scattering, the difference in obtained thermal conductivity is less than 7% at 300 K with the iterative solution of the BTE. The obtained thermal conductivity is converged to within 5% with these choices of numerical parameters (phonon wavevector grid, interaction cutoffs, etc.).

4. Results

The experimentally measured lattice constants of ThO_2 are 5.592 Å and 5.600 Å as reported respectively by Hirata et al. [53] and by Idiri et al. [54], when measured at room temperature. In comparison, our DFT relaxed lattice constants are 5.519 Å, 5.613 Å, and 5.556 Å using the LDA, PBE, and PBEsol functionals. Considering that ThO_2 undergoes negligible thermal expansion at 300 K [55], our DFT-obtained lattice constants are in good agreement with the experiments. Consequently, for temperature range 100 K–320 K, we do not include any thermal expansion while for 1000 K, we included thermal expansion of 0.6% [55] in our reported results.

The phonon dispersions of ThO_2 as obtained using the lowest-order theory with temperature-independent force constants (OK-FC) are reported in Fig. 2(a). For comparison, the experimentally measured phonon frequencies, as reported by Clausen et al. [48] and Bryan et al. [15], are also plotted in the same figure. We find that for the acoustic phonons, the frequencies obtained from the considered three functionals are similar and are in agreement with the experimentally reported frequencies. However, for low [high] frequency optical modes with a frequency range 5–12 THz [12–20 THz], PBEsol [LDA] functional results in better agreement with experimental measurements. This is coherent with results presented by Dennet et al. where authors also reported good agreement of experimental data with LDA functional [16].

With the inclusion of tdep and renorm, the acoustic modes remain unchanged. The optical modes, however, undergo stiffening in the entire frequency range, as presented in Figs. 2(b), 2(c), and 2(d) for LDA, PBE, and PBEsol functionals respectively. Consequently, while the obtained acoustic mode frequencies are in agreement with experiments for all three functionals, the optical phonons show better agreement for PBE functional with the inclusion of higher-order effects. Nevertheless, considering that only low-frequency acoustic modes are active at room temperature, the thermal transport is expected to be well described by all three functionals in ThO_2 at and below room temperatures.

The phonon scattering rates, obtained by considering 3ph and 4ph scattering processes, are reported in Fig. 3 for ThO_2 at 300 K. The results reported in Fig. 3 are obtained using the PBE functional and the results are similar from LDA and PBEsol functionals. At 300 K, we find that while there are differences for low-frequency optical phonons, the obtained scattering rates of heat-carrying acoustic phonons are similar with and without 4ph scattering. In particular, at 300 K, the phonon thermal conductivity obtained by including 4ph scattering differs by less than 9% for all three functionals, compared to that obtained by considering only the 3ph scattering. As such, considering that 4ph scattering is expected to have a lesser effect at lower temperatures, it is not included in the thermal conductivities reported in the subsequent sections for room temperature and below.

The phonon thermal conductivity obtained by considering tdep and renorm is reported in Fig. 4 along with experimentally reported results of Mann et al. [11] and Dennet et al. [16] for single crystal samples. We find that PBE functional under-predicts thermal conductivity of the single-crystal samples for the entire temperature range. This is despite an excellent agreement of PBE functional predicted phonon dispersion with experimental results. Further, while there is a minimal variation

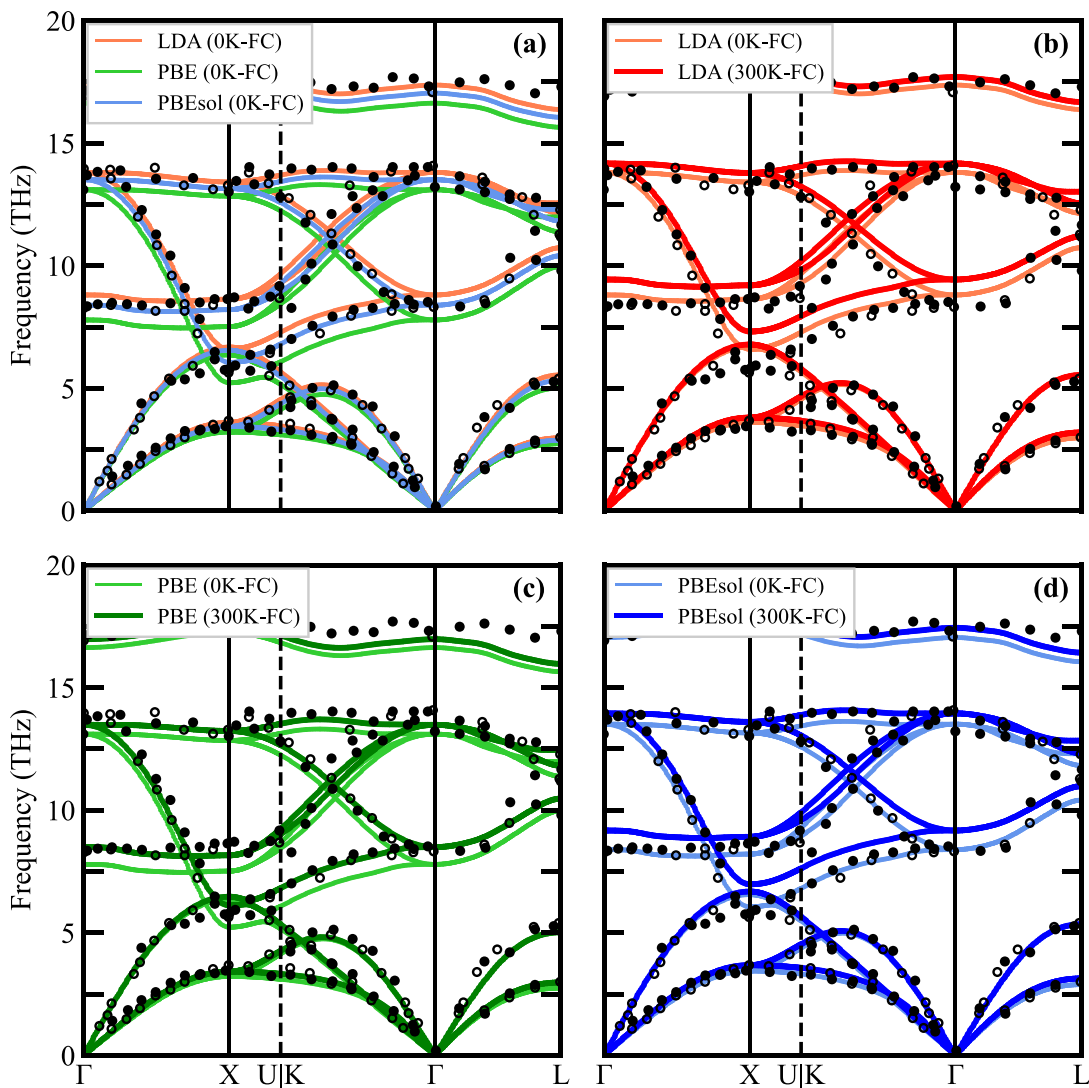


Fig. 2. Phonon Dispersion of ThO_2 . (a) The comparison of phonon dispersions obtained using the lowest-order thermal transport physics by employing the LDA, PBE, and PBEsol functionals. The effect of temperature on phonon dispersion is reported in (b), (c), and (d) for LDA, PBE, and PBEsol functionals. The open and filled circles represent inelastic neutron scattering measurement data from Clausen et al. (at 293 K) [48] and Bryan et al. (at 300 K) [15].

in acoustic phonon dispersion across different functionals [the speed of sound, i.e., the longitudinal acoustic phonon group velocity in the 100 direction is 6166, 6023, and 6120 m/s from LDA, PBE, and PBEsol functionals], the obtained thermal conductivities from LDA and PBEsol functionals are within 5% of the experimentally measured value at 300 K while that obtained from PBE functional is an under-prediction of 25%. This lower value of thermal conductivity obtained from PBE functional is a consequence of the wrong description of anharmonicity by PBE functional as can be seen from the phonon lifetimes computed by the three functionals (Fig. 5). Noticeably, below 5 THz (where the major contribution to lattice thermal conductivity is observed), the PBE functional under-predicts phonon lifetimes compared to LDA and PBEsol functionals.

In Fig. 4, the deviations between experiments and computations (LDA, PBEsol) at lower temperatures could be due to the presence of visible defects in the crystal sample used for measurements by Mann et al. [11], which leads to phonon-defect scattering and reduced thermal conductivity at lower temperatures. The effect of reduction in measured thermal conductivity at lower temperatures due to impurity scattering is evident from another set of single crystal experimental measurements made by Dennet et al. [16], in which the sample material had higher impurity concentration.

From Fig. 3, it is apparent that the 4ph scattering has an effect on the phonon lifetimes for low-frequency optical phonons at 300 K. With increasing temperature, the 4ph scattering is expected to get more pronounced. To highlight the significance of 4ph scattering and other higher-order effects at high temperatures, we report the thermal properties of ThO_2 obtained using the LDA functional at 300 K and 1000 K in Fig. 6. A lattice thermal expansion of 0.6% (as reported by Touloukian et al. [55]) is considered while carrying out calculations at 1000 K. We find that the difference in lattice thermal conductivity computed from the conventional (lower-level thermal transport physics) method and the higher-level thermal transport physics are 10% and 27% when computed using LDA functional at 300 K and 1000 K respectively. However, the reduction in lattice thermal conductivity solely by 4ph scattering processes are less than 7% and 10% at these temperatures.

5. Concluding remarks

To conclude, we studied the effect of the inclusion of higher-order thermal transport physics on the first-principles-based lattice dynamics calculations of phonon frequencies and lattice thermal conductivity of pristine ThO_2 . We find that the renormalization of phonon frequencies results in the stiffening of the optical phonon modes, whereas the

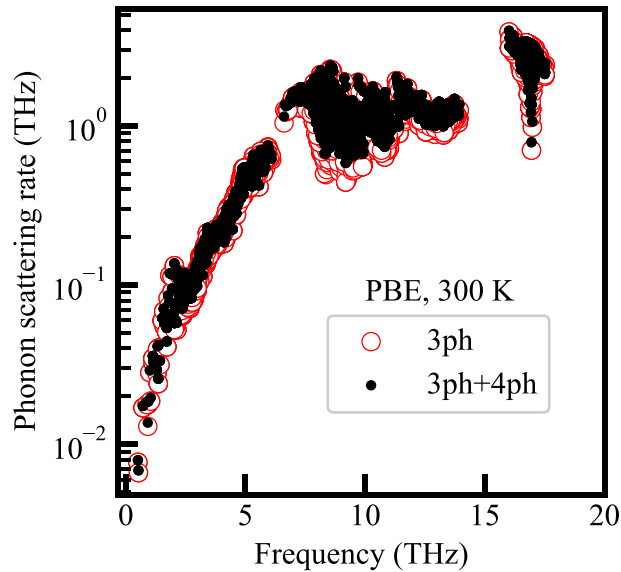


Fig. 3. Phonon Scattering Rates. The scattering rates of phonons as obtained using only 3ph (red) and 3ph+4ph scatterings (black) at 300 K using the PBE functional by employing the higher-order thermal transport physics.

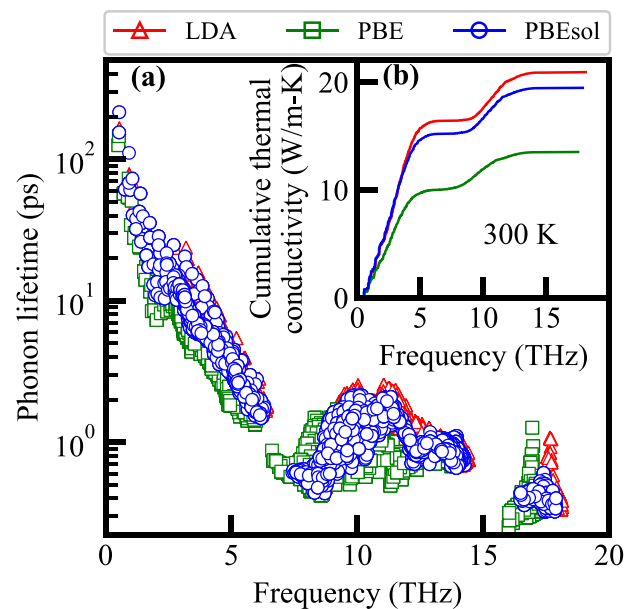


Fig. 5. Effect of XC functional on Mode-dependent Phonon Properties. (a) Phonon lifetimes and (b) cumulative thermal conductivity at 300 K, obtained using LDA, PBE, and PBEsol functionals incorporating higher-order thermal transport physics.

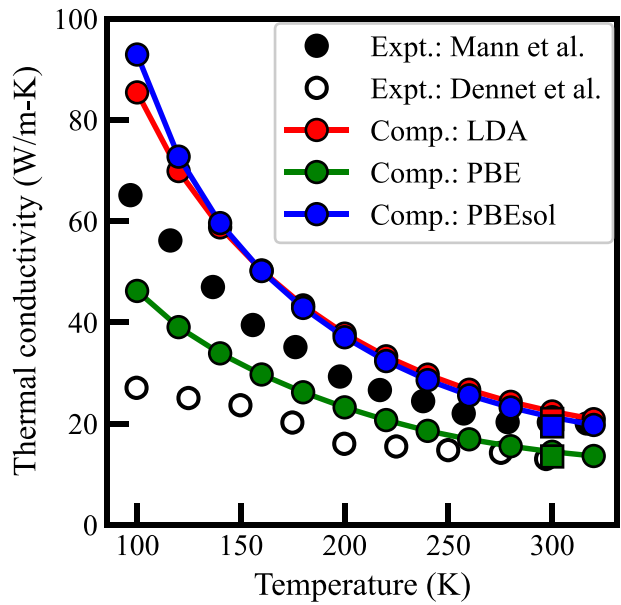


Fig. 4. Temperature-dependent Phonon Thermal Conductivity. The temperature-dependent thermal conductivities of ThO_2 as obtained using the LDA, PBE, and PBEsol functionals by considering higher-order thermal transport effects (tdep and renorm). The 4ph scattering is included only at 300 K and is denoted using square symbols. Experimental datasets are from Mann et al. [11] and Dennet et al. [16].

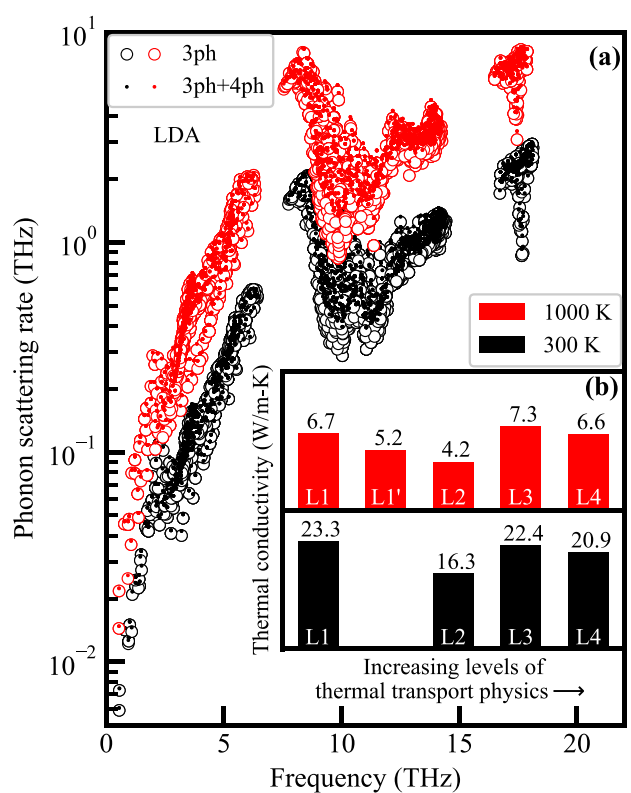


Fig. 6. Phonon Properties at 1000 K. (a) Phonon scattering rates at 300 K and 1000 K obtained by considering only 3ph (open circles) and 3ph+4ph (dots) processes with LDA functional, and (b) Effect of various higher-order thermal transport physics on the obtained phonon thermal conductivity at 300 K and 1000 K: L1 indicates the conventional lower-level thermal transport physics (OK-FC & 3ph), L1' incorporates the effects of thermal expansion on top of L1, and L2, L3, and L4 successively incorporates the effect of tdep, renorm, and 4ph.

renormalization change in frequencies for acoustic modes was minimal. The acoustic mode frequencies obtained using the LDA, PBE, and PBEsol XC functionals agree well with experimental data, whereas the low-frequency optical modes are better described by PBE functional. The PBE functional resulted in an underprediction of phonon lifetimes, and consequently the lattice thermal conductivity; whereas thermal conductivities obtained using the LDA and PBEsol functionals agreed well with the experimental measurements. The inclusion of tdep and

renorm showed a significant increase in computed thermal conductivity at higher temperatures compared to that computed using temperature-independent calculations (40% at 1000 K). The 4ph processes have minimal effect on the computed lattice thermal conductivity for ThO₂ even at 1000 K and can be ignored to save the computational cost.

CRediT authorship contribution statement

Nidheesh Virakante: Writing – original draft, Visualization, Validation, Software, Methodology, Investigation, Formal analysis, Data curation. **Ankit Jain:** Writing – review & editing, Supervision, Resources, Project administration, Methodology, Investigation, Funding acquisition, Conceptualization.

Declaration of competing interest

The authors declare that they have no known competing financial interests or personal relationships that could have appeared to influence the work reported in this paper.

Acknowledgments

The authors acknowledge the financial support from the Core Research Grant, Science & Engineering Research Board, India (Grant No. CRG/2021/000010) and Nano Mission, Government of India (Grant Number : DST/NM/NS/2020/340). The calculations were carried out on the SpaceTime-II supercomputing facility of IIT Bombay and PARAM Porul (located at NIT Trichy, India) supercomputing facility provided by the Centre for Development of Advanced Computing (CDAC).

Data availability

Data will be made available on request.

References

- [1] David H. Hurley, Anter El-Azab, Matthew S. Bryan, Michael W.D. Cooper, Cody A. Dennett, Krzysztof Gofryk, Lingfeng He, Marat Khafizov, Gerard H. Lander, Michael E. Manley, et al., Thermal energy transport in oxide nuclear fuel, *Chem. Rev.* 122 (3) (2021) 3711–3762.
- [2] Linu Malakkal, Anil Prasad, Ericmoore Jossou, Jayangani Ranasinghe, Barbara Szpunar, Lukas Bichler, Jerzy Szpunar, Thermal conductivity of bulk and porous tho₂: Atomistic and experimental study, *J. Alloys Compd.* 798 (2019) 507–516.
- [3] J. Stephen Herring, Uranium and thorium resources, in: Nuclear Energy: Selected Entries from the Encyclopedia of Sustainability Science and Technology, Springer, 2012, pp. 463–490.
- [4] Wei Zhou, Wenzhong Zhou, Enhanced thermal conductivity accident tolerant fuels for improved reactor safety—a comprehensive review, *Ann. Nucl. Energy* 119 (2018) 66–86.
- [5] Paul Van Uffelen, Jason Hales, W. Li, G. Rossiter, Richard Williamson, A review of fuel performance modelling, *J. Nucl. Mater.* 516 (2019) 373–412.
- [6] Masayuki Murabayashi, Thermal conductivity of ceramic solid solutions, *J. Nucl. Sci. Technol.* 7 (11) (1970) 559–563.
- [7] P. Srirama Murti, C.K. Mathews, Thermal diffusivity and thermal conductivity studies on thorium-lanthanum mixed oxide solid solutions, *J. Phys. D: Appl. Phys.* 24 (12) (1991) 2202.
- [8] K. Bakker, E.H.P. Cordfunke, R.J.M. Konings, R.P.C. Schram, Critical evaluation of the thermal properties of tho₂ and thl- ypu₀₂, *J. Nucl. Mater.* 250 (1) (1997) 1–12.
- [9] C.G.S. Pillai, P. Raj, Thermal conductivity of tho₂ and tho_{0.98}u_{0.02}o₂, *J. Nucl. Mater.* 277 (1) (2000) 116–119.
- [10] Jae Ho Yang, Ki Won Kang, Kun Woo Song, Chan Bock Lee, Youn Ho Jung, Fabrication and thermal conductivity of (th, u) o₂ pellets, *Nucl. Technol.* 147 (1) (2004) 113–119.
- [11] Matthew Mann, Daniel Thompson, Karn Serivalsatit, Terry M. Tritt, John Ballato, Joseph Kolis, Hydrothermal growth and thermal property characterization of tho₂ single crystals, *Cryst. Growth & Des.* 10 (5) (2010) 2146–2151.
- [12] Bao-Tian Wang, Hongliang Shi, Wei-Dong Li, Ping Zhang, First-principles study of ground-state properties and high pressure behavior of tho₂, *J. Nucl. Mater.* 399 (2–3) (2010) 181–188.
- [13] Yong Lu, Yu Yang, Ping Zhang, Thermodynamic properties and structural stability of thorium dioxide, *J. Phys.: Condens. Matter.* 24 (22) (2012) 225801.
- [14] Jianye Liu, Zhenhong Dai, Xiuxian Yang, Yinchang Zhao, Sheng Meng, Lattice thermodynamic behavior in nuclear fuel tho₂ from first principles, *J. Nucl. Mater.* 511 (2018) 11–17.
- [15] Matthew S. Bryan, Lyuwen Fu, Karl Rickert, David Turner, Timothy A. Prusnick, J. Matthew Mann, Douglas L. Abernathy, Chris A. Marianetti, Michael E. Manley, Nonlinear propagating modes beyond the phonons in fluorite-structured crystals, *Commun. Phys.* 3 (1) (2020) 217.
- [16] Cody A. Dennett, W. Ryan Deskins, Marat Khafizov, Zilong Hua, Amey Khanolkar, Kaustubh Bawane, Lyuwen Fu, J. Matthew Mann, Chris A. Marianetti, Lingfeng He, et al., An integrated experimental and computational investigation of defect and microstructural effects on thermal transport in thorium dioxide, *Acta Mater.* 213 (2021) 116934.
- [17] W. Ryan Deskins, Ahmed Hamed, Tomohisa Kumagai, Cody A. Dennett, Jie Peng, Marat Khafizov, David Hurley, Anter El-Azab, Thermal conductivity of tho₂: Effect of point defect disorder, *J. Appl. Phys.* 129 (7) (2021).
- [18] Miaomiao Jin, Marat Khafizov, Chao Jiang, Shuxiang Zhou, Chris A. Marianetti, Matthew S. Bryan, Michael E. Manley, David H. Hurley, Assessment of empirical interatomic potential to predict thermal conductivity in tho₂ and uo₂, *J. Phys.: Condens. Matter.* 33 (27) (2021) 275402.
- [19] W. Ryan Deskins, Amey Khanolkar, Sanjoy Mazumder, Cody A. Dennett, Kaustubh Bawane, Zilong Hua, Joshua Ferrigno, Lingfeng He, J. Matthew Mann, Marat Khafizov, et al., A combined theoretical-experimental investigation of thermal transport in low-dose irradiated thorium dioxide, *Acta Mater.* 241 (2022) 118379.
- [20] Enda Xiao, Hao Ma, Matthew S. Bryan, Lyuwen Fu, J. Matthew. Mann, Barry Winn, Douglas L. Abernathy, Raphaël P. Hermann, Amey R. Khanolkar, Cody A. Dennett, et al., Validating first-principles phonon lifetimes via inelastic neutron scattering, *Phys. Rev. B* 106 (14) (2022) 144310.
- [21] Weiqiang Wang, Yinchang Zhao, Jun Ni, Sheng Meng, Zhenhong Dai, Ab initio investigations on lattice dynamics and thermal transport properties of tho₂, *Mater. Chem. Phys.* 307 (2023) 128138.
- [22] Hiroki Nakamura, Masahiko Machida, First-principles calculation study on phonon thermal conductivity of thorium and plutonium dioxides: Intrinsic anharmonic phonon-phonon and extrinsic grain-boundary–phonon scattering effects, *J. Nucl. Mater.* 519 (2019) 45–51.
- [23] Nidheesh Virakante, Ankit Jain, Considerations for ab-initio based thermal conductivity prediction of tho₂, in: Proceedings of the 27th National and 5th International ISHMT-ASTFE Heat and Mass Transfer Conference, December 14–17, 2023, IIT Patna, Patna-801106, Bihar, India, Begel House Inc., 2024.
- [24] Jungkyu Park, Eduardo B. Farfán, Christian Enriquez, Thermal transport in thorium dioxide, *Nucl. Eng. Technol.* 50 (5) (2018) 731–737.
- [25] Miaomiao Jin, Cody A. Dennett, David H. Hurley, Marat Khafizov, Impact of small defects and dislocation loops on phonon scattering and thermal transport in tho₂, *J. Nucl. Mater.* 566 (2022) 153758.
- [26] Ziqiang Wang, Chen Yang, Miaozen Yu, Wenzhong Ma, Liyao Guo, Zhixian Wei, Ning Gao, Zhongwen Yao, Xuelin Wang, Effect of fission products on the thermal conductivity of tho₂-a molecular dynamics study, *Nucl. Mater. Energy* (2024) 101681.
- [27] Charles Kittel, Paul McEuen, *Introduction to Solid State Physics*, John Wiley & Sons, 2018.
- [28] P.G. Klemens, The thermal conductivity of dielectric solids at low temperatures (theoretical), *Proc. R. Soc. Lond. Ser. A. Math. Phys. Sci.* 208 (1092) (1951) 108–133.
- [29] Micheline Roufosse, P.G. Klemens, Thermal conductivity of complex dielectric crystals, *Phys. Rev. B* 7 (12) (1973) 5379.
- [30] D.A. Broido, T.L. Reinecke, Lattice thermal conductivity of superlattice structures, *Phys. Rev. B—Condens. Matter Mater. Phys.* 70 (8) (2004) 081310.
- [31] Asegun S. Henry, Gang Chen, Spectral phonon transport properties of silicon based on molecular dynamics simulations and lattice dynamics, *J. Comput. Theor. Nanosci.* 5 (2) (2008) 141–152.
- [32] L. Lindsay, D.A. Broido, Optimized tersoff and brenner empirical potential parameters for lattice dynamics and phonon thermal transport in carbon nanotubes and graphene, *Phys. Rev. B—Condens. Matter Mater. Phys.* 81 (20) (2010) 205441.
- [33] Shuxiang Zhou, Chao Jiang, Enda Xiao, Michael W.D. Cooper, Miaomiao Jin, Chris A. Marianetti, David H. Hurley, Marat Khafizov, Improving empirical interatomic potentials for predicting thermophysical properties by using an irreducible derivatives approach: The case of thorium dioxide, 2022, arXiv preprint arXiv:2204.13685.
- [34] Alan J.H. McGaughey, Ankit Jain, Hyun-Young Kim, Bo Fu, Phonon properties and thermal conductivity from first principles, lattice dynamics, and the boltzmann transport equation, *J. Appl. Phys.* 125 (1) (2019).
- [35] Lucas Lindsay, First principles Peierls-Boltzmann phonon thermal transport: a topical review, *Nanoscale Microscale Thermophys. Eng.* 20 (2) (2016) 67–84.
- [36] Ping Zhang, Bao-Tian Wang, Xian-Geng Zhao, Ground-state properties and high-pressure behavior of plutonium dioxide: Density functional theory calculations, *Phys. Rev. B—Condens. Matter Mater. Phys.* 82 (14) (2010) 144110.
- [37] John M. Ziman, *Electrons and Phonons: The Theory of Transport Phenomena in Solids*, Oxford University Press, 2001.
- [38] J.A. Reissland, The Physics of Phonons, A Wiley-Interscience Publication. Wiley, ISBN: 9780471715856, 1973, <https://books.google.co.in/books?id=kgdRAAAAMAAJ>.

- [39] Ankit Jain, Multichannel thermal transport in crystalline tl_3vse_4 , Phys. Rev. B 102 (2020) 201201, <http://dx.doi.org/10.1103/PhysRevB.102.201201>, URL <https://link.aps.org/doi/10.1103/PhysRevB.102.201201>.
- [40] Ankit Jain, Impact of four-phonon scattering on thermal transport in carbon nanotubes, Phys. Rev. B 109 (2024) 155413, <http://dx.doi.org/10.1103/PhysRevB.109.155413>, URL <https://link.aps.org/doi/10.1103/PhysRevB.109.155413>.
- [41] K. Esfarjani, G. Chen, H.T. Stokes, Heat transport in silicon from first-principles calculations, Phys. Rev. B 84 (2011) 085204.
- [42] L. Lindsay, D.A. Broido, T.L. Reinecke, $\langle \rangle_{\text{ab initio}}$ thermal transport in compound semiconductors, Phys. Rev. B 87 (2013) 165201, <http://dx.doi.org/10.1103/PhysRevB.87.165201>, URL <http://link.aps.org/doi/10.1103/PhysRevB.87.165201>.
- [43] Ankit Jain, Alan J.H. McGaughey, Strongly anisotropic in-plane thermal transport in single-layer black phosphorene, Sci. Rep. 5 (2015) <http://dx.doi.org/10.1038/srep08501>, URL <http://www.nature.com/srep/2015/150217/srep08501/abs/srep08501.html#supplementary-information>.
- [44] Ankit Jain, Alan J.H. McGaughey, Effect of exchange–correlation on first-principles-driven lattice thermal conductivity predictions of crystalline silicon, Comput. Mater. Sci. 110 (2015) 115–120.
- [45] Navaneetha K. Ravichandran, David Broido, Unified first-principles theory of thermal properties of insulators, Phys. Rev. B 98 (8) (2018) 085205.
- [46] Tianli Feng, Lucas Lindsay, Xiulin Ruan, Four-phonon scattering significantly reduces intrinsic thermal conductivity of solids, Phys. Rev. B 96 (16) (2017) 161201.
- [47] D. West, S.K. Estreicher, First-principles calculations of vibrational lifetimes and decay channels: $\langle \rangle$ hydrogen-related modes in si, Phys. Rev. Lett. 96 (11) (2006) 115504.
- [48] Kurt Clausen, William Hayes, J Emryr Macdonald, Ray Osborn, Peter G. Schnabel, Michael T. Hutchings, Andreas Magerl, Inelastic neutron scattering investigation of the lattice dynamics of tho 2 and ceo 2, J. Chem. Soc. Faraday Trans. 2: Mol. Chem. Phys. 83 (7) (1987) 1109–1112.
- [49] Paolo Giannozzi, Stefano Baroni, Nicola Bonini, Matteo Calandra, Roberto Car, Carlo Cavazzoni, Davide Ceresoli, Guido L. Chiarotti, Matteo Cococcioni, Ismaila Dabo, et al., Quantum espresso: a modular and open-source software project for quantum simulations of materials, J. Phys.: Condens. Matter. 21 (39) (2009) 395502.
- [50] Paolo Giannozzi, Oliviero Andreussi, Thomas Brumme, Oana Bunau, M. Buongiorno Nardelli, Matteo Calandra, Roberto Car, Carlo Cavazzoni, Davide Ceresoli, Matteo Cococcioni, et al., Advanced capabilities for materials modelling with quantum espresso, J. Phys.: Condens. Matter. 29 (46) (2017) 465901.
- [51] Peter E. Blöchl, Projector augmented-wave method, Phys. Rev. B 50 (24) (1994) 17953.
- [52] Stefano Baroni, Stefano De Gironcoli, Andrea Dal Corso, Paolo Giannozzi, Phonons and related crystal properties from density-functional perturbation theory, Rev. Modern Phys. 73 (2) (2001) 515.
- [53] Koichi Hirata, K. Moriya, Y. Waseda, High temperature thermal expansion of $\text{tho}_{2/3}$, mgo and $\text{y}_{2/3}\text{o}_{3/2}$ by x-ray diffraction, J. Mater. Sci.;(United Kingdom) 12 (4) (1977).
- [54] M. Idiri, T. Le Bihan, S. Heathman, Jean Rebizant, Behavior of actinide dioxides under pressure: uo_2 and th o_2 , Phys. Rev. B—Condens. Matter Mater. Phys. 70 (1) (2004) 014113.
- [55] Y.S. Touloukian, R.K. Kirby, R.E. Taylor, T.Y.R. Lee, IFI/Plenum, Thermal expansion: Nonmetallic solids, in: Thermophysical Properties of Matter, IFI/Plenum, 1970, <https://books.google.co.in/books?id=Rt9p0AEACAAJ>.